Mansoura Engineering Journal

Volume 48 | Issue 4 Article 2

2023

Experimental Study of Photovoltaic Performance Under a Compound Parabolic Solar Concentrator with a Nanofluid Spectral Filter

O. Elharoun
Mechanical Power Engineering Department, Faculty of Engineering, Mansoura University, El-Mansoura 35516, Egypt

M. Tawfik
Mechanical Power Engineering Department, Faculty of Engineering, Mansoura University, El-Mansoura 35516, Egypt, m_tawfik@mans.edu.eg

Ibrahim I. El-Sharkawy
Mechanical Power Engineering Department, Faculty of Engineering, Mansoura University, El-Mansoura 35516, Egypt

E. Zeidan
Mechanical Power Engineering Department, Faculty of Engineering, Mansoura University, El-Mansoura 35516, Egypt

ORIGINAL STUDY

Experimental Study of Photovoltaic Performance Under a Compound Parabolic Solar Concentrator with a Nanofluid Spectral Filter

Omar Elharoun [a], Mohamed Tawfik [a,*], Ibrahim I. El-Sharkawy [b,a], El-Shafei Zeidan [a]

[a] Mechanical Power Engineering Department, Faculty of Engineering, Mansoura University, El-Mansoura, 35516, Egypt
[b] Sustainable and Renewable Energy Engineering Department, College of Engineering, University of Sharjah, Sharjah, 27272, United Arab Emirates

Abstract

The spectral-splitting technique splits the sun's spectrum into two pieces to save photovoltaic cells from overheating. The first component is instantly converted into electricity, while the second is used to generate heat energy. Since nanofluid simultaneously serves as a heat transfer liquid and a spectrum splitter, several investigations have demonstrated that it is a very effective liquid-based filter. This work presents a novel PV/T design incorporating a compound parabolic concentrator (CPC) and a ZnO-water nanofluid filter over the PV cell. In this work, different ZnO concentrations, such as 50, 100, 150, and 200 ppm, were tested to assess their impact on system performance. The average results were then compared to those of a reference PV cell. The results showed that the percentage reduction in PV cells' temperature rises steadily with concentration, from 9.9% at 50 ppm to 10.7% at 200 ppm. Moreover, the average enhancement percentages in electrical power and efficiency increase consistently from 88% to 89.3%—93% and 107.5%, respectively, as the nanofluid's concentration climbs from 50 ppm to 200 ppm. In contrast, the electrical efficiency of filtered cells rises from 7.1% at 50 ppm to 7.7% at 100 ppm before falling to 6.7% and 6.2% at 150 ppm and 200 ppm, respectively. The thermal and overall efficiencies steadily rise with concentration, climbing from 27.9% to 31.7% at 50 ppm to 31.4% and 34.6% at 200 ppm, respectively.

Keywords: Compound parabolic concentrator, Efficiency, Photovoltaic, Solar, Spectral filtration

1. Introduction

A significant portion of the heat, light, and power required to sustain life on earth comes from solar energy. With high efficiencies and no need for noisy, complicated systems, PV cells have recently become the most effective way to convert sunlight into electricity directly. The primary problem with PV systems is the rise in temperature during operation, which reduces efficiency since the semiconductor material can only convert solar light with the proper spectral response for the PV cell, while the rest is converted to heat. This problem is well-solved by spectral-splitting technology, which excludes UV and IR radiation that would otherwise cause the PV cell to overheat and only allows solar energy compatible with the PV cell's spectral response to reach the cell. These technologies can be classified into many groups, such as reflective-based (Mojiri et al., 2013), absorbed-based (Wang et al., 2022), and diffractive and refractive-based (Xiao et al., 2016). Many studies have shown that nanofluid can simultaneously act as a heat transfer fluid and a spectral splitter, making it an effective liquid-based filter. Huaxu et al. (2020) investigated the effect of the ZnO nanoparticle concentration in glycol on electrical and thermal performances. When particle concentration was increased from 11.2 ppm to 89.2 ppm, thermal efficiency increased by 47%. The electrical efficiency, however,

Received 10 December 2022; revised 4 April 2023; accepted 11 May 2023.
Available online 26 June 2023

* Corresponding author at: Mansoura University Faculty of Engineering, Mansoura, Dakahliya, Egypt. Tel./fax: +2 050 2202248.
E-mail address: m_tawfik@mans.edu.eg (M. Tawfik).

https://doi.org/10.58491/2735-4202.3049

decreased. In a study presented by Hjerrild et al. (2016) to test the effect of different CNTs-water and Ag−SiO_2 nanofluid concentrations, Ag−SiO_2 filters with a concentration of 0.026 wt% boosted combined efficiencies by 30% when contrasted with just the base fluid filter. An also studied the effect of particle concentration, Zhang et al. (An et al., 2016a), and the findings showed that while the thermal efficiency dropped with increasing particle concentration, the temperature of the nanofluid and the electrical efficiency rose. The performance of a PV/T system based on an Ag−$CoSO_4$ nanofluid spectral filter was proposed by Han et al. (2019). The findings demonstrate that when Ag nanoparticle mass fractions are equal, Ag/$CoSO_4$ nanofluid exhibits stronger visible and UV wavelength absorption than a water-based one.

Moreover, at the same mass fraction of Ag nanoparticles, Ag/$CoSO_4$ nanofluids have a lower electrical output than Ag/water nanofluids but have a greater stagnation temperature. He, Hu, and Li's study (He et al., 2019) used ethylene glycol/water solution (3:2, v/v) as the base fluid because of its low freezing point and suitability for cold areas. It was possible to achieve an overall efficiency of up to 83.7% at 1 kWm^{-2} with Ag@TiO_2 nanoparticle concentrations as low as 200 ppm. This extraordinary performance was mainly attributable to wideband light absorption, which produces a sizable thermal energy. Li et al. (2019) found that the 200 ppm Ag@TiO_2-water nanofluid's overall efficiency was around 1.4 times greater than water's. The maximum total efficiency of the PV/T system designed by An, Wu et al. (An et al., 2016b) based on Cu_9S_5-Oleylamine nanofluid was 34.2%, 17.9% more than the unfiltered system. Using a blend of indium tin oxide and gold nanoparticles in Duratherm S, Otanicar et al.'s system (Otanicar et al., 2018) achieved a maximum thermal efficiency of 61% with a fluid output temperature of 110 °C and an electric efficiency of 4% at a concentration ratio of 14. The PV/T system could create 12% more power than a bare PV cell under the same sunlight, according to an experimental study by Crisostomo et al. (2017), utilizing Ag−SiO_2-water nanofluid. The thermal conductivity and the transmittance of silica/water nanofluids of different particle sizes were examined by Jing et al. (2015). The findings demonstrated that the transmittance of nanofluids with a particle diameter of 5 nm and volume fractions of 2% could reach as high as 97%, which is quite near that of pure water. A 20% improvement in this nanofluid's thermal conductivity was also observed. To address the shortcomings of solar distillation systems, a more advanced system that combines a PV/T system with spectral-splitting nanofluids was developed by An et al. (2018). The upgraded systems with Ag and Au nanoparticles had a thermal efficiency gain of 4.8% and 6.8%, respectively. Additionally, the system's electrical efficiency with Ag-nanofluid was higher than Au-nanofluid's.

As explained in the previous literature, nanofluids have proven their effectiveness as liquid-based absorbed filters, where the effect of different types of nanoparticles with different concentrations and different types of liquids with different properties on the electrical and thermal performance of the system has been studied. Despite this, previous studies did not study the performance and stability of the system over hours in which the intensity of solar radiation changes throughout the day, as the system performance was only tested for several minutes. In addition, the system performance was not tested when integrating a compound parabolic solar concentrator to concentrate solar radiation with the PV/T system. This work suggests a novel PV/T design that combines a compound parabolic concentrator (CPC) with a ZnO-water nanofluid, a selective absorptive filter over the PV cell. To test the effect of various ZnO-water nanofluid concentrations of 50, 100, 150, and 200 ppm (0.05, 0.1, 0.15, and 0.2 kg/m^3) on the system's performance, many tests were conducted over a comparable 4.5-h time span from 10:30 to 15:00 on several days. After that, the average results were compared.

2. Experimental setup

The setup for the experiment is depicted in Fig. 1. It was executed at Mansoura University in Mansoura, Egypt (31.0449°N, 31.3537°E). Several experiments were carried out over a more extended period, from September 4 to October 5, to examine the increase in performance while utilizing varied concentrations of ZnO nanofluid. The research presented here proposes a unique PV/T system that combines a compound parabolic concentrator (CPC) with a ZnO-water nanofluid that acts as a selective absorptive filter over the PV cell. Several experiments were carried out during a comparable 4.5-h period from 10:30 to 15:00 on several different days to examine the impact of different ZnO-water nanofluid concentrations of 50, 100, 150, and 200 ppm (0.05, 0.1, 0.15, and 0.2 kg/m^3)on the system's performance.

The system consists of a CPC (1) with a 30° tilt that faces south. The significant reflectivity of nickel-chrome made it the ideal choice for a reflecting substance. The wooden block (2) was made by stacking many identically sized and shaped layers of

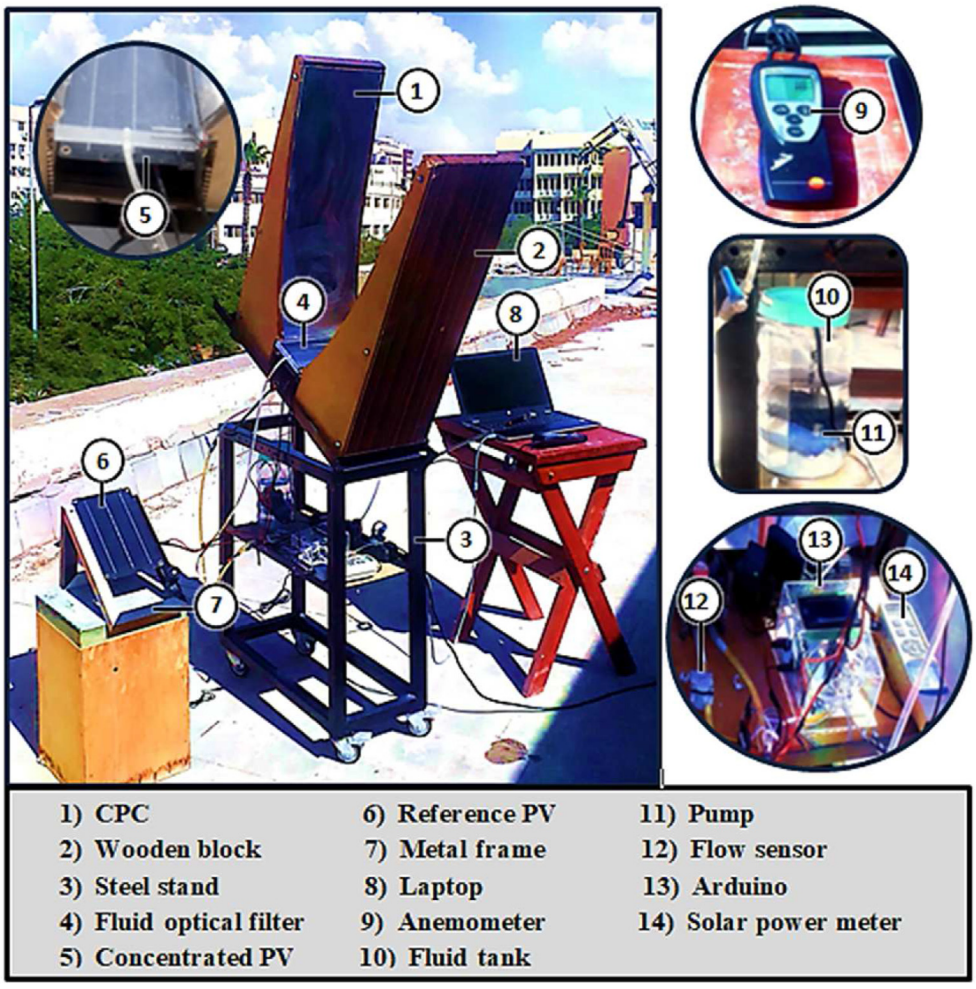

Fig. 1. Experimental setup.

MDF and was attached to the CPC using glue. The CPC is made up of two symmetric parabolas. The lower end of any parabola is the focal point of the other (Bahaidarah et al., 2014), as indicated in Fig. 2. The angle created by the axes of the two parabolas, known as the half-acceptance angle, is crucial for designing CPCs. As shown in Fig. 3, only radiation that is incident at an angle less than or equal to the half-acceptance angle $(\theta_i \leq \theta_a)$ may be reflected on the absorber; all other radiation is reflected back into the aperture.

The geometrical concentration ratio (CR) is the proportion of the exit area to the aperture area. Its relationship to the half-acceptance angle is demonstrated by Equation (1) (Zheng, 2017) as follows:

$$CR = \frac{1}{\sin \theta_a} = \frac{W_{ap}}{W_{ab}} \tag{1}$$

Where W_{ab} , W_{ap} are the absorber and aperture widths, respectively. The upper portion of the CPC was trimmed to a third of its original length, which lowered the cost of the reflective material. Equation (2) provides the height for the whole CPC prior to truncation (Zheng, 2017):

$$H_{CPC} = \frac{f \cos \theta_a}{\sin^2 \theta_a} = 0.5 W_{ab}(CR+1)\sqrt{CR^2-1} \tag{2}$$

where f is the CPC parabola's focal length, which is determined by Equation (3) (Zheng, 2017) as follows:

$$f = 0.5\, W_{ab}(1+\sin \theta_a) \tag{3}$$

Equation (4) provides the height of the concentrator after trimming (Zheng, 2017) as follows:

$$H_{CPC,T} = \frac{0.5\, W_{ap,T}(1+\sin \theta_a)\cos(\theta_{c,T}-\theta_a)}{\sin(\theta_{c,T}-\theta_a)(1+\sin \theta_a) - \sin^2(\theta_{c,T}/2)} \tag{4}$$

Where $W_{ap,T}$ is the width of the aperture after truncation, $\theta_{c,T}$ is the angle of concentration after

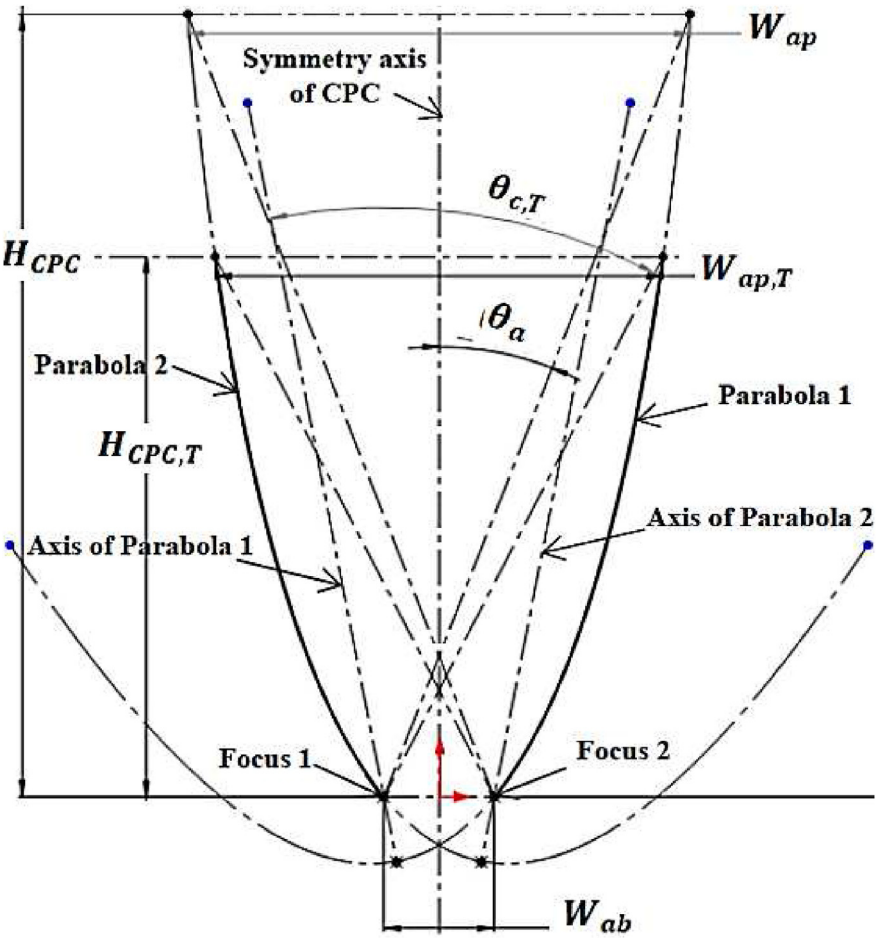

Fig. 2. The geometry of CPC.

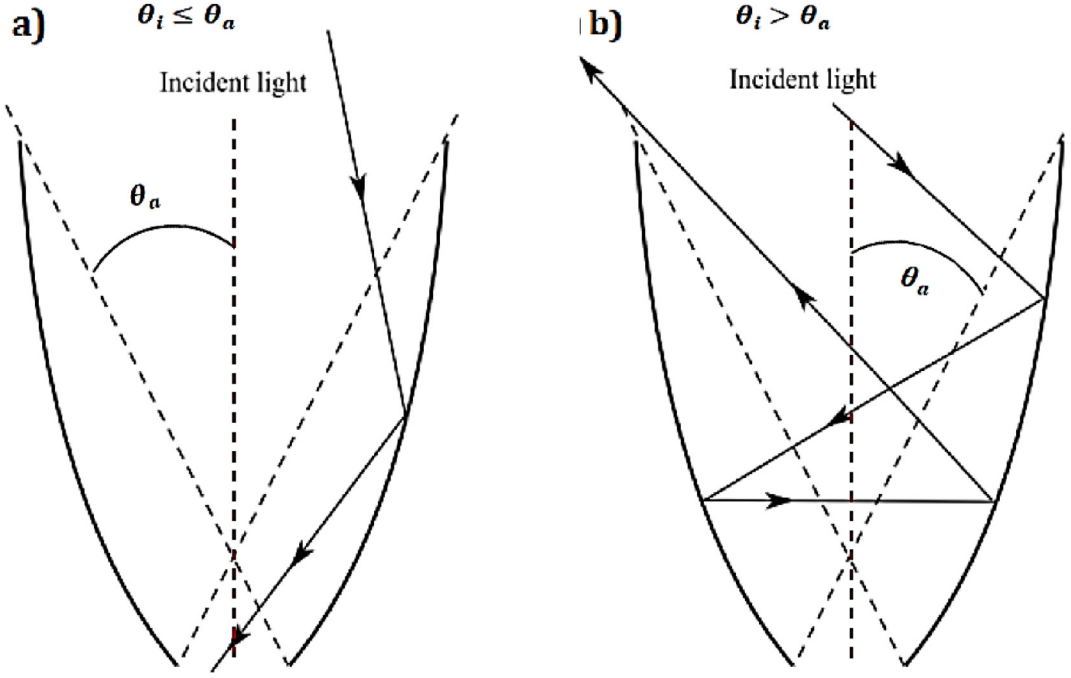

Fig. 3. The paths of incident radiation on the CPC.

Table 1. PV cell characteristics under standard test circumstances (I_{ref} = 1000 W/m^2, $T_{PV,ref}$ = 25°C and AM_{ref} = 1.5).

Parameter	Value
The current at maximum power, I_{mp}	1 A
The voltage at maximum power, V_{mp}	6 V
The maximum power, P_{mp}	6 W
The short circuit current, I_{sc}	1.1 A
The open circuit voltage, V_{oc}	7.2 V

truncation. The CPC's concentration ratio after truncation is given by Equation (5) (Zheng, 2017) as follows:

$$CR_T = \frac{W_{ap,T}}{W_{ab}} = \frac{f \sin(\theta_{c,T} - \theta_a)}{0.5\, W_{ab} \sin^2(\theta_{c,T}/2)} - 1 = \frac{(1 + \sin\theta_a)\sin(\theta_{c,T} - \theta_a)}{\sin^2(\theta_{c,T}/2)} - 1 \quad (5)$$

As a result of truncation, the CPC concentration ratio in the current study is reduced to 4. The width of the aperture after truncation can be related to that before truncation by Equation (6) as follows (Zheng, 2017):

$$W_{ap,T} = \frac{2f \sin(\theta_{c,T} - \theta_a)}{\sin^2(\theta_{c,T}/2)} - W_{ab} \quad (6)$$

A rectangular fluid-based optical filter (4) with a thickness of 0.01 m was made using acrylic (PMMA) slaps. The wooden block's bottom grooves regulate the distance between the concentrated PV cell (5) and the liquid channel. To compare the performance to that of the concentrated cell, a reference PV cell (6) with the exact dimensions (0.275 × 0.155 m) was placed up next to the wooden block on a metal frame (7). A pump (11) circulated the nanofluid in a closed loop, with a valve regulating the flow rate. A water flow sensor (12) measuring a range of 0.3–6 l/min (5×10^{-6}–10^{-4} m^3/s) was used to gauge the flow rate. A solar power meter (14) records the sun's irradiance every 10 s. The wind speed is measured using a vane anemometer (9). Digital thermometers were used to gauge the temperatures of PMMA channels, PV cells, and ambient air. Waterproof sensors were used to gauge the temperature of the fluid at the channels' entrance and outflow. Each sensor is connected to an Arduino microcontroller unit (13), which logs measurements to a memory card every 3 s. The cells' current and voltage were also recorded every 3 s. Both an LCD affixed to the Arduino box and a laptop (8) was used to display all the data regularly. The specifications of both PV cells under standard conditions are listed in Table 1. Detailed information about the measuring tools employed in the experimental research is listed in Table 2.

3. Nanofluid preparation

In the current work, ZnO nanofluid samples were created using the two-step process (Huaxu et al., 2020; Vidhya et al., 2021) at varying concentrations of 50, 100, 150, and 200 ppm (0.05, 0.1, 0.15, and 0.2 kg/m^3). The nanoparticles are first created and added to the primary solution in this method. First, samples of ZnO nanoparticles with average diameters of 30 nm were introduced to 1 L of pure water. These samples had weights of 0.05, 0.1, 0.15, and 0.2 g. Then, for 20 min, with one pulse every two seconds, the solution was stirred by an ultrasonic liquid processor [SONICS (Vibra-cell) MODEL: CV334], as shown in Fig. 4, with a maximum output power of 750 W and a frequency of 20 kHz.

The amount of solar radiation that may effectively travel through the nanofluid to the cell without causing PV overheating is greatly influenced by the spectral transmittance of the nanofluid, which is computed by Equation (7) as follows (Han et al., 2019; Yazdanifard et al., 2020):

$$\tau_{\lambda,nf} = exp\left(-\sigma_{nf} \cdot e_{nf}\right) \quad (7)$$

Where e_{nf} is the nanofluid channel thickness, σ_{nf} is the extinction coefficient of nanofluid, which is the summation of nanoparticles and base fluid extinction coefficients as illustrated by Equation (8), Equation (9), and Equation (10) as follows (Taylor et al., 2011, 2012):

Table 2. Detailed information about the measuring tools employed in this study.

Measured value	Tool	Accuracy	Ref.
Wind speed	Testo 416––Small vane anemometer	±0.2 m/s	(Vane Anemometer (Testo 416), 2022)
Solar radiation	Solar power meter (SPM-1116SD)	±10 W/m^2	SOLAR POWER METER Model: SPM-1116SD (1116)
Flow rate	Water Flow Sensor (YF–S401)	±2%	High Precision PVC Water Flow Sensor YF-S401 (2022)
Liquid temperature	Waterproof sensor (DS18B20)	±0.5 °C	(Waterproof Te mperature Sensor Cable (DS18B20), 1420)
PV cell, PMMA, and ambient air temperatures	Digital Thermometer (DS18B20-PAR)	±0.5 °C	(Digital Thermometer (DS18B20-PAR), 1576)
Current and voltage	Current and Voltage Sensor (MAX471)	±2%	Max471/Max472 (2022)

Fig. 4. Nanofluid preparation using ultrasonic liquid processor.

$$\sigma_{ext} = \sigma_{\mathrm{np}} + \sigma_{\mathrm{bf}} \tag{8}$$

$$\sigma_{\mathrm{bf}} = 4\pi \frac{\kappa_{\mathrm{bf}}}{\lambda} \tag{9}$$

$$\sigma_{\mathrm{np}} = \frac{3}{2} \frac{\varnothing_v (\eta_{sc} + \eta_{abs})}{D_{np}} \tag{10}$$

Where κ_{bf} is the base fluid's absorption index, D_{np} is the nanoparticle's average diameter, which for the ZnO particles utilized in this work is equivalent to 30 nm. $\varnothing_v$ is the nanoparticles' volume fraction, which is given by Equation (11). η_{sc} and η_{abs} are the nanoparticles' scattering and absorption efficiencies, which can be given by Equation (12) and Equation (13), respectively (Yazdanifard et al., 2020; Jing and Song, 2017), as follows:

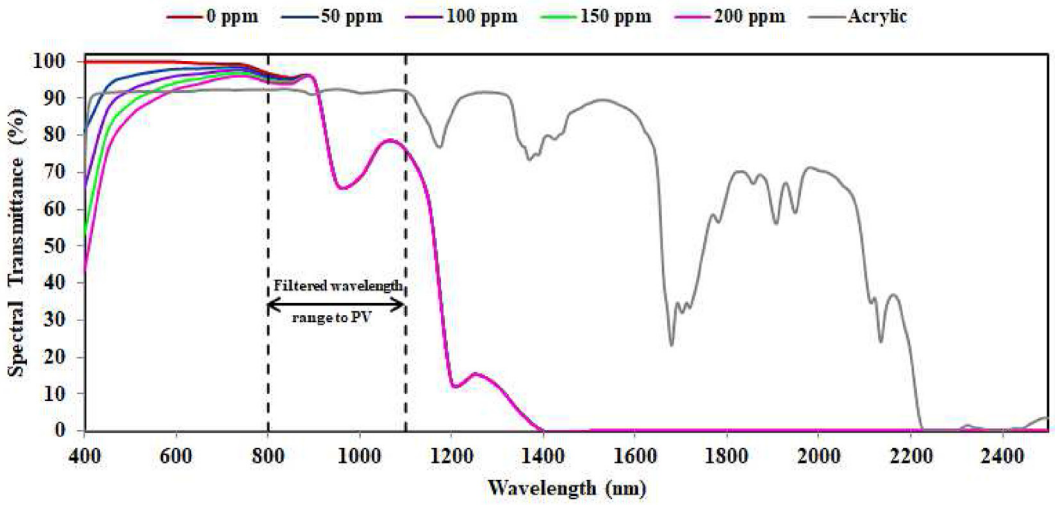

Fig. 5. The spectral transmittances of the 3 mm thick acrylic slab and the 0.01 m thick ZnO-water nanofluid for different concentrations.

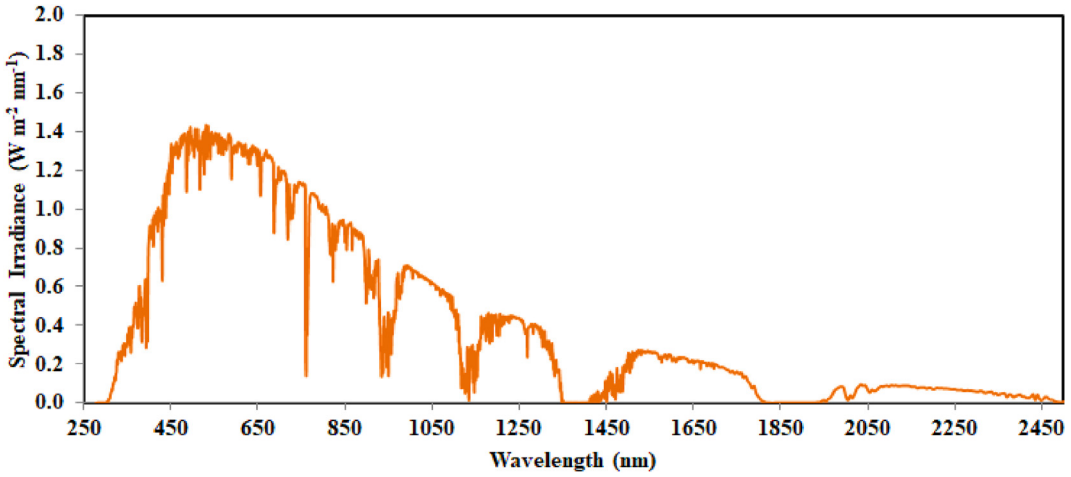

Fig. 6. Solar spectral irradiance at AM = 1.5.

$$\varnothing_v = \frac{\frac{m_{np}}{\rho_{np}}}{\frac{m_{bf}}{\rho_{bf}} + \frac{m_{np}}{\rho_{np}}} \tag{11}$$

$$\eta_{sc} = \frac{8}{3} S_{np}^4 \cdot Re\left[\left(\frac{R^2-1}{R^2+2}\right)^2\right] \tag{12}$$

$$\eta_{ab} = 4 S_{np} Im\left\{\frac{R^2-1}{R^2+2}\left[1 + \frac{S_{np}^2}{15}\left(\frac{R^2-1}{R^2+2}\right)\frac{R^4+27R^2+38}{2R^2+3}\right]\right\} \tag{13}$$

m_{bf}, m_{np} are the masses of the base fluid and nanoparticles, respectively. ρ_{bf}, ρ_{np} are the densities of the base fluid and nanoparticles, respectively. R is the nanofluid's complex refractive index, which is the ratio between the complex refractive indices of the nanoparticles and base fluid, as illustrated by Equation (14). The nanoparticle size parameter, S_{np}, is determined by Equation (15) based on Rayleigh scattering approximation that is valid when S_{np}"1 and $|R|S_{np}$"1.

$$R = \frac{R_{np}}{R_{\mathrm{bf}}} = \frac{n_{np} + i\kappa_{np}}{n_{\mathrm{bf}} + i\kappa_{\mathrm{bf}}} \tag{14}$$

Table 3. Average transmittances of the optical filter throughout various wavelength bandwidths.

Nanofluid concentration (ppm)	Average transmittance (%)			
	(400–2500) nm	(400–800) nm	(800–1100) nm	(1100–2500) nm
0 ppm	64.8	81.4	72.5	5.5
50 ppm	63.1	78.9		
100 ppm	61.6	76.3		
150 ppm	60.2	74		
200 ppm	58.9	71.9		

$$S_{np} = \frac{\pi D_{np}}{\lambda} \tag{15}$$

n_{bf}, n_{np} are the base fluid's and nanoparticles' refraction indices, respectively. κ_{bf}, κ_{np} are the absorption indices of the base fluid and nanoparticles, respectively. Several research papers derived these indices for water (Hale and Querry, 1973; Otanicar et al., 2009) and ZnO nanoparticles (Huaxu et al., 2019; Royanian et al., 2020; Zarandi and Bioki, 2017; Manoharan et al., 2016) at various wavelengths.

4. Results and discussion

4.1. The impact of nanofluid concentration on spectral transmittance

The monocrystalline PV cell utilized in this work should receive solar radiation with energy close to the silicon band gap energy (1.12 eV). The matching wavelength of this band gap, according to studies (Huaxu et al., 2020; He et al., 2019), is close to 1100 nm. Therefore, most thermal radiation has wavelengths longer than 1100 nm and belongs to the infrared (IR) spectrum, which cannot produce electrical power because its energy is lower than the silicon band gap. Conversely, wavelengths shorter than 1100 nm have more energy than the silicon band gap; as a result, only some of this energy is converted into electricity, while

Table 4. Dates of each concentration test.

Date	Testing Interval	Nanofluid concentration (ppm)
5/09/2022	10:30–15:00	50
6/09/2022		100
18/09/2022		200
5/10/2022		150

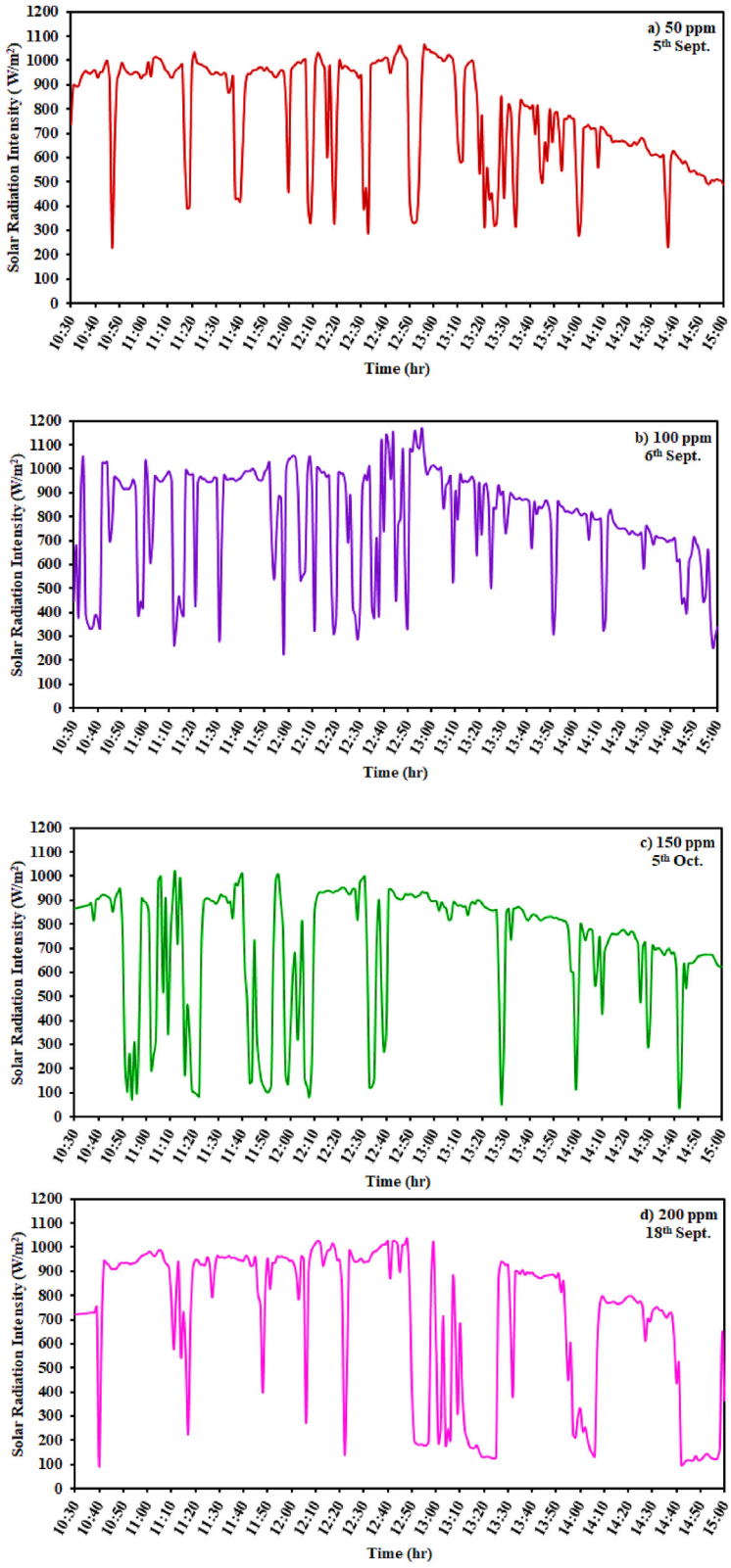

Fig. 7. Solar radiation intensity for different concentration experiments.

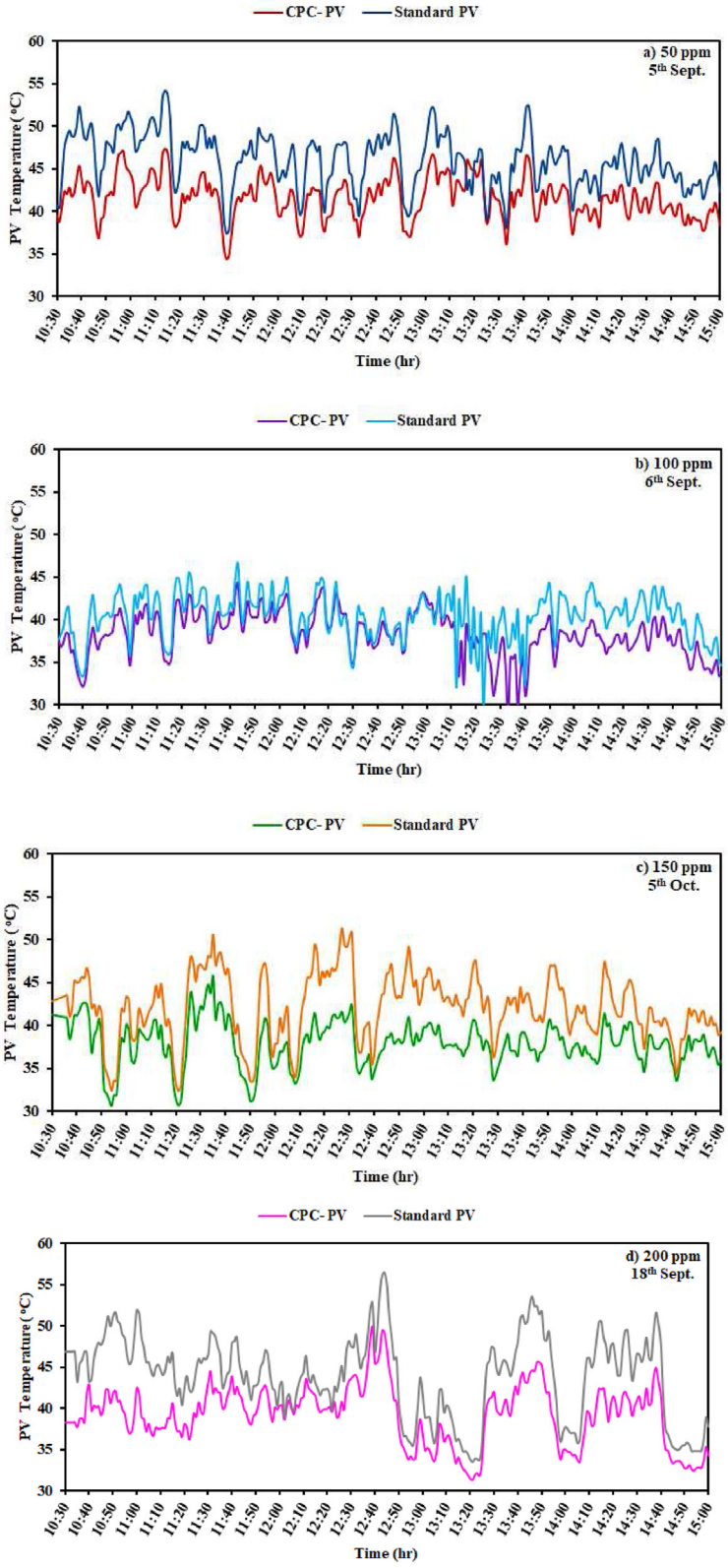

Fig. 8. Average concentrated and reference PV temperature curves for all tested cases.

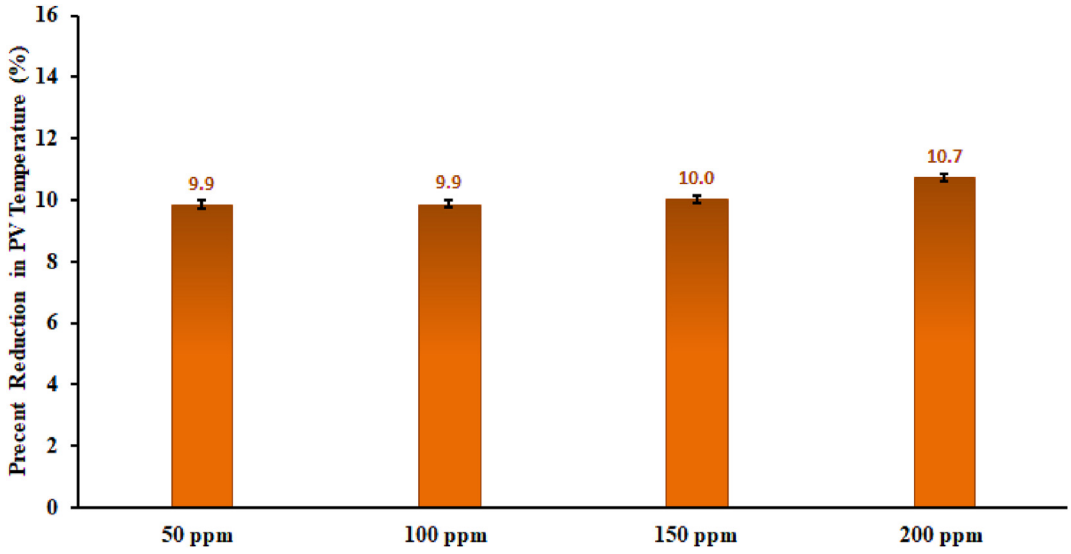

Fig. 9. Comparison of average filtered PV temperature reduction for all tested cases.

the remainder raises the cell's temperature and lowers its efficiency. Therefore, the optical filter should block all sunlight with energy below the silicon band gap energy, which implies blocking wavelengths longer than 1100 nm.

Additionally, a portion of solar irradiance with energy higher than the silicon band gap (wavelengths below 800 nm (Saroha et al., 2015; Rodrigues Fernandes and Schaefer, 2019)) should also be blocked. The spectral transmittance of ZnO-water nanofluid can be determined for different concentrations of ZnO-nanoparticles using Equations (7)–(25). Fig. 5 displays the spectral transmittance of ZnO-water nanofluid for concentrations of 0, 50, 100, 150 and 200 ppm with a fluid layer thickness of 0.01 m. The spectral transmittance of the 3 mm thick acrylic slab is also indicated in Fig. 5 (Molded Plastic Aspheric Lenses, 2022).

The spectral transmittance of ZnO-water nanofluid decreases with concentration below a wavelength of 800 nm. However, it practically remains constant above it, as seen in Fig. 5. The average transmittance of the whole optical filter (0.01 m nanofluid layer and two 3 mm acrylic layers) can be calculated by the following equation:

$$\tau_{of} = \frac{\int_{400\ nm}^{2500\ nm} I_\lambda \tau_{\lambda,ac}^2 \tau_{\lambda,nf}\, d\lambda}{\int_{400\ nm}^{2500\ nm} I_\lambda\, d\lambda} \tag{16}$$

Where $\tau_{\lambda,nf}$ is the nanofluid's spectral transmittance, $\tau_{\lambda,ac}$ is the acrylic's spectral transmittance, I_λ is the solar spectral irradiance, which is plotted in Fig. 6 at AM = 1.5 based on typical values [(ASTM G-173-03) (ISO 9845-1, 1992) (NREL(Reference Air Mass 1.5 Spectra), 2022)] defined for solar concentrator work. Table 3 provides the average transmittances of optical filters throughout the various wavelength bandwidths.

As shown in Table 3, the optical filter's average transmittance declines gradually over the wavelength range of (400–2500 nm), from 81.4% at 0 ppm to 71.9% at 200 ppm, while it remains nearly constant over the wavelength ranges of (800–1100 nm) and (1100–2500 nm), with average values of 72.5% and 5.5%, respectively.

4.2. The comparison of the CPC-PV system with a nanofluid optical filter against the reference PV cell for various concentrations

Since only a fraction of the sun's light is converted into electricity and the rest raises the solar cell's temperature, the solar cell temperature is highly dependent on the amount of solar radiation that enters the system. Therefore, various experiments were carried out on September 5th, 6th, 18th, and October 5. Table 4 lists the dates and the corresponding concentrations of nanofluid. The four testing days' solar radiation is plotted in Fig. 7. Fig. 8 displays the average concentrated and reference PV temperature curves for all tested cases.

As illustrated in Fig. 8, there is an apparent reduction in PV cell average temperature owing to the effect of solar spectral filtration. Therefore, to compare all the tested cases, the drop in concentrated cell average temperature can be expressed as a percentage as follows:

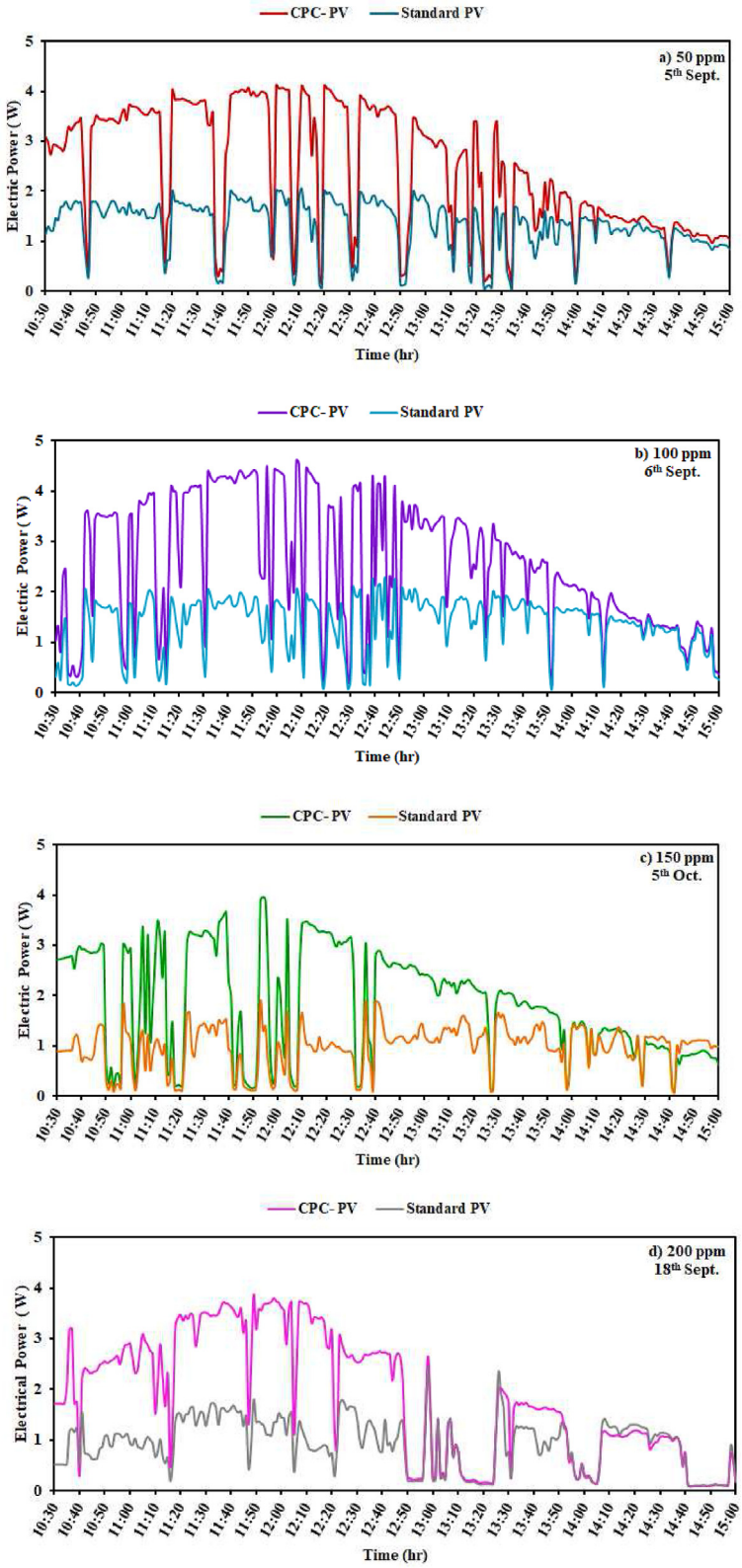

Fig. 10. The output power variation with time for all tested cases.

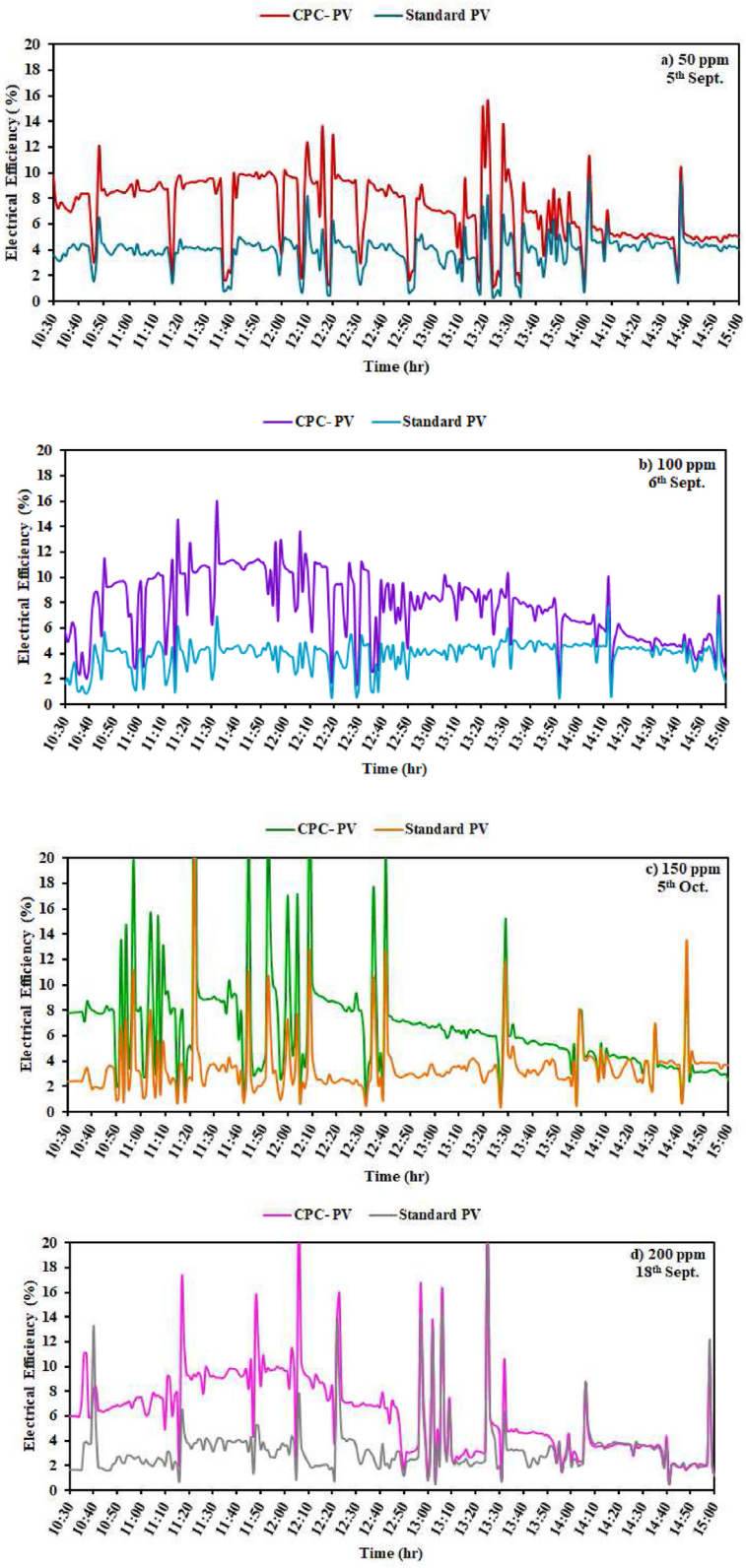

Fig. 11. The variation of electrical efficiency with time for all tested cases.

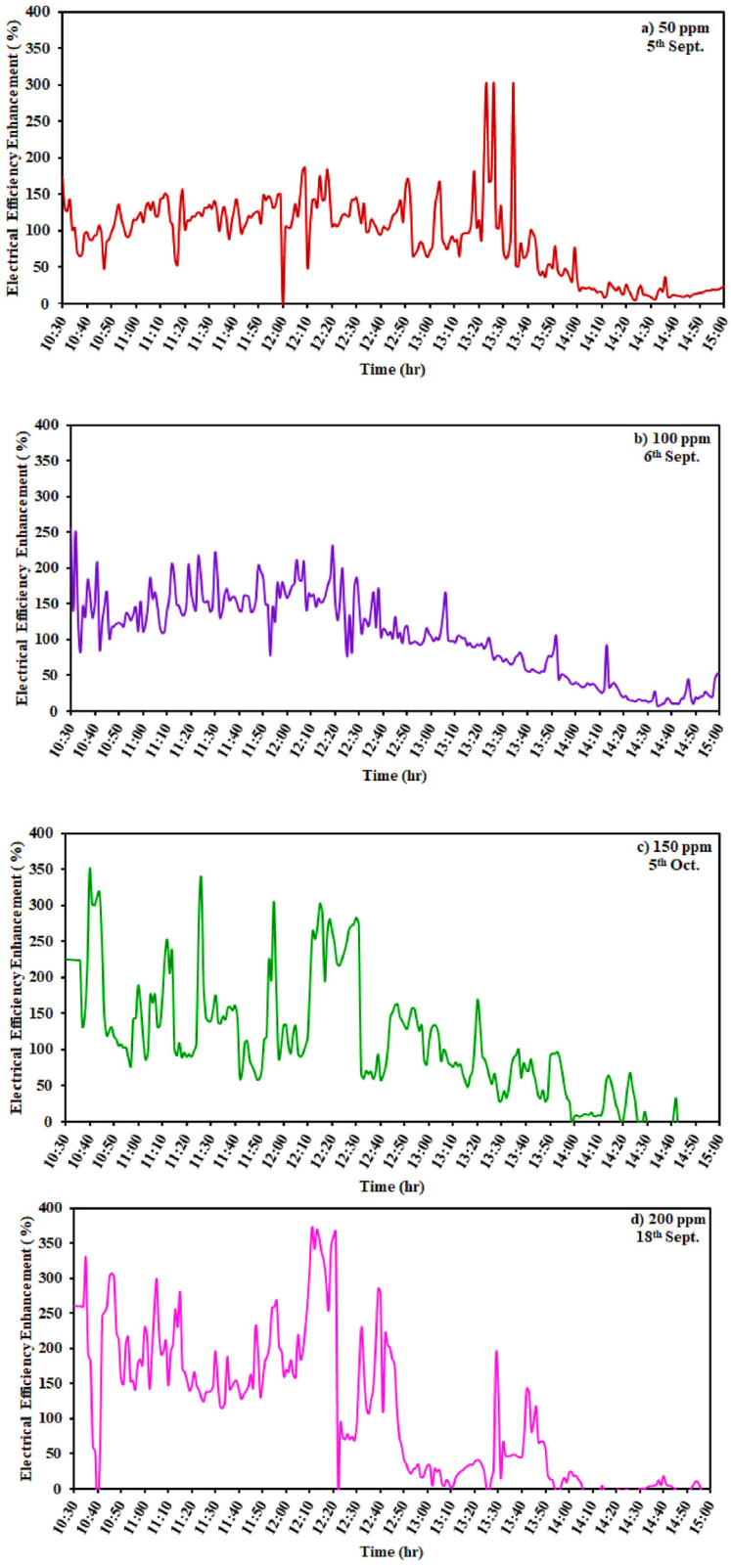

Fig. 12. The variations in electrical efficiency improvement percentages over time for all studied cases.

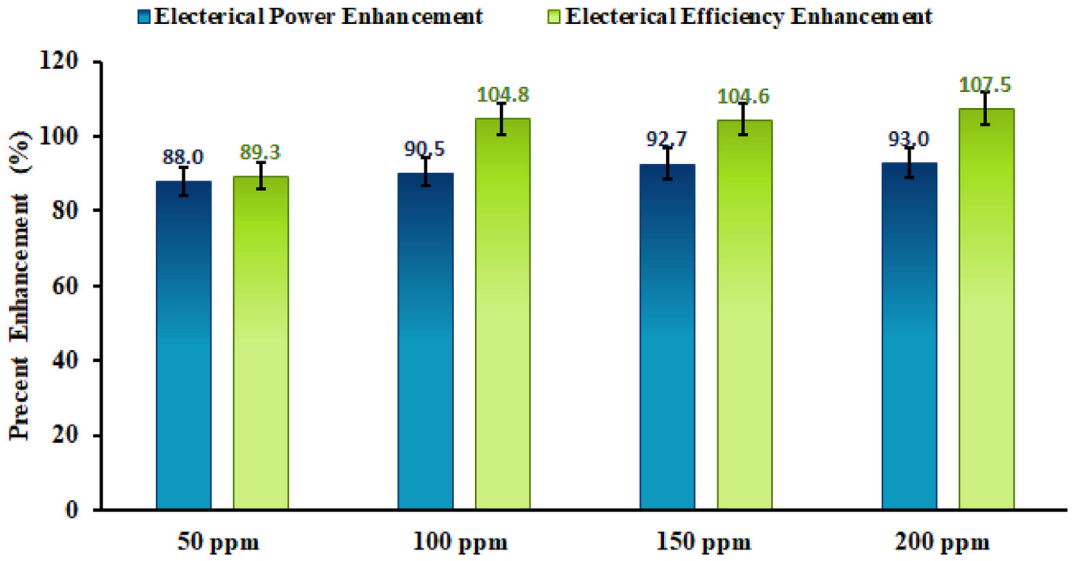

Fig. 13. A comparison of the average percent increase in electrical power and efficiency for all studied cases.

$$\textit{Reduction percentage in average PV temperature}\ \% = \frac{\sum_{j=1}^{n_t} \frac{\overline{T_{PV,ref_j}} - \overline{T_{PV_j}}}{\overline{T_{PV,ref_j}}}}{n_t} * 100 \tag{17}$$

Where $\overline{T_{PV_j}}$ and $\overline{T_{PV,ref_j}}$ are the concentrated and reference cells' average temperatures at any moment, respectively. n_t is the total number of time steps over the testing interval where the data was captured every 3 s. According to Fig. 9, which compares the percentage reduction in filtered cell average temperature for all investigated situations, a gradual increase in percent reduction is obtained from 9.9% at a nanofluid concentration of 50 ppm to 10.7% at a concentration of 200 ppm.

In comparison to the reference systems, Fig. 10 shows the increased electric power of the filtered systems over the tested period compared to the reference cell. The reference cell's electrical efficiency, $\eta_{PV,ref}$, and that of the filtered systems, η_{PV} , can be calculated as follows (Adam et al., 2019):

$$\eta_{PV,ref} = \frac{I\,V}{I_{ab} A_{ab}} \tag{18}$$

$$\eta_{PV} = \frac{I\,V}{I_{ab} A_{ab} \tau_{ac}^2 \tau_{nf}} \tag{19}$$

Where, V are the measured output current and voltage of the PV cell, I_{ab} is the absorbed solar radiation by the cell, A_{ab} is the solar cell's surface area, τ_{ac} is the average transmittance of the acrylic layer, τ_{nf} is the nanofluid's average transmittance. Fig. 11 displays the variations in electrical efficiency with time for the filtered PV systems and the reference PV cells for all nanofluid concentrations.

The electrical power and efficiency enhancement percentages owing to using the nanofluid filter can be expressed by the following equations:

$$\textit{Electric power enhancement}\ \% = \frac{\sum_{j=1}^{n_t} \frac{P_{PV,ref_j} - P_{PV_j}}{P_{PV,ref_j}}}{n_t} * 100 \tag{20}$$

$$\textit{Electrical efficiency enhancement}\ \% = \frac{\sum_{j=1}^{n_t} \frac{\eta_{PV,ref_j} - \eta_{PV_j}}{\eta_{PV,ref_j}}}{n_t} * 100 \tag{21}$$

Where P_{PV_j} , P_{PV,ref_j} are the filtered and reference cell's electric power at any time from the start, respectively. η_{PV_j}, η_{PV,ref_j} are the filtered and reference cell's electric efficiency at any time from the start, respectively. Fig. 12 displays the variations in electrical efficiency improvement percentages over time for all studied cases. The boost in all cases is

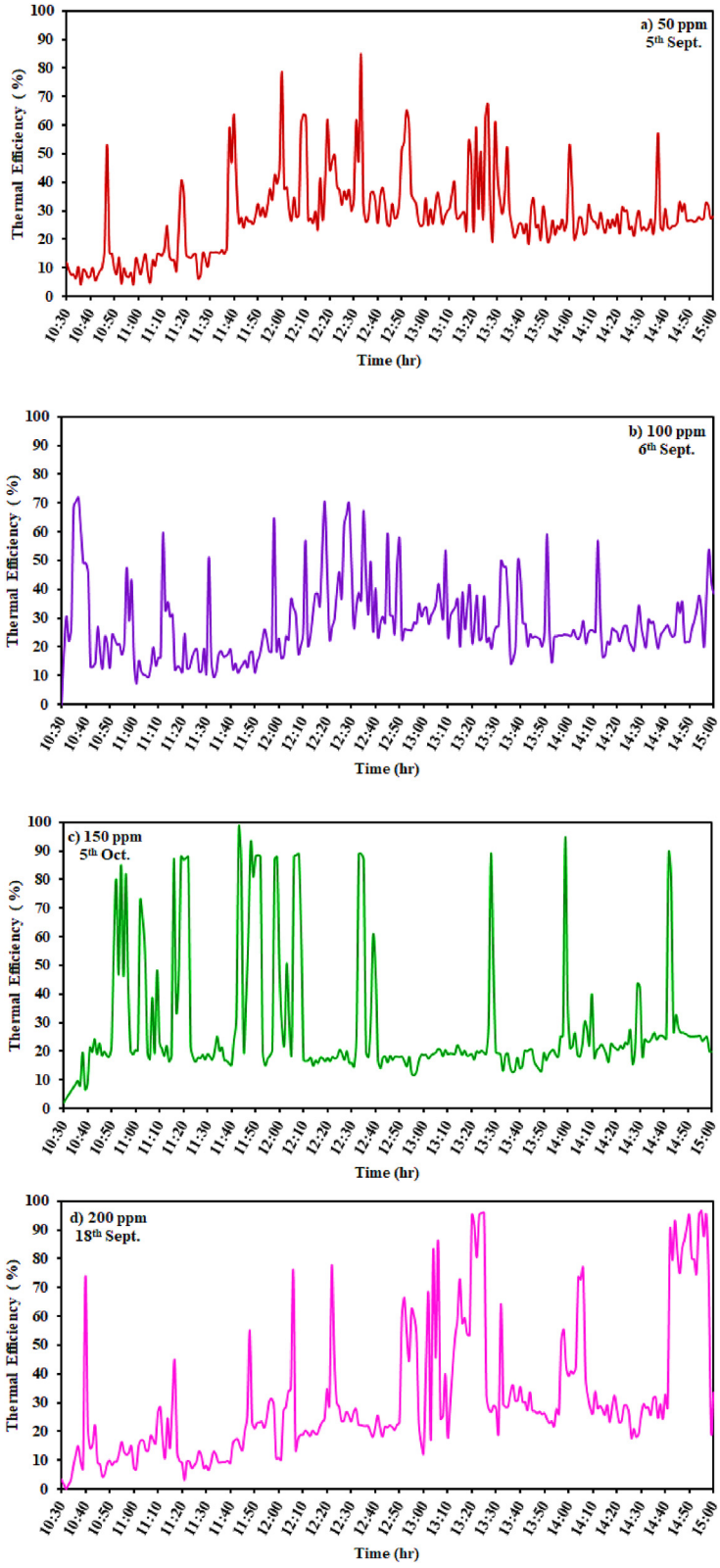

Fig. 14. The variation of thermal efficiency over time for all studied cases.

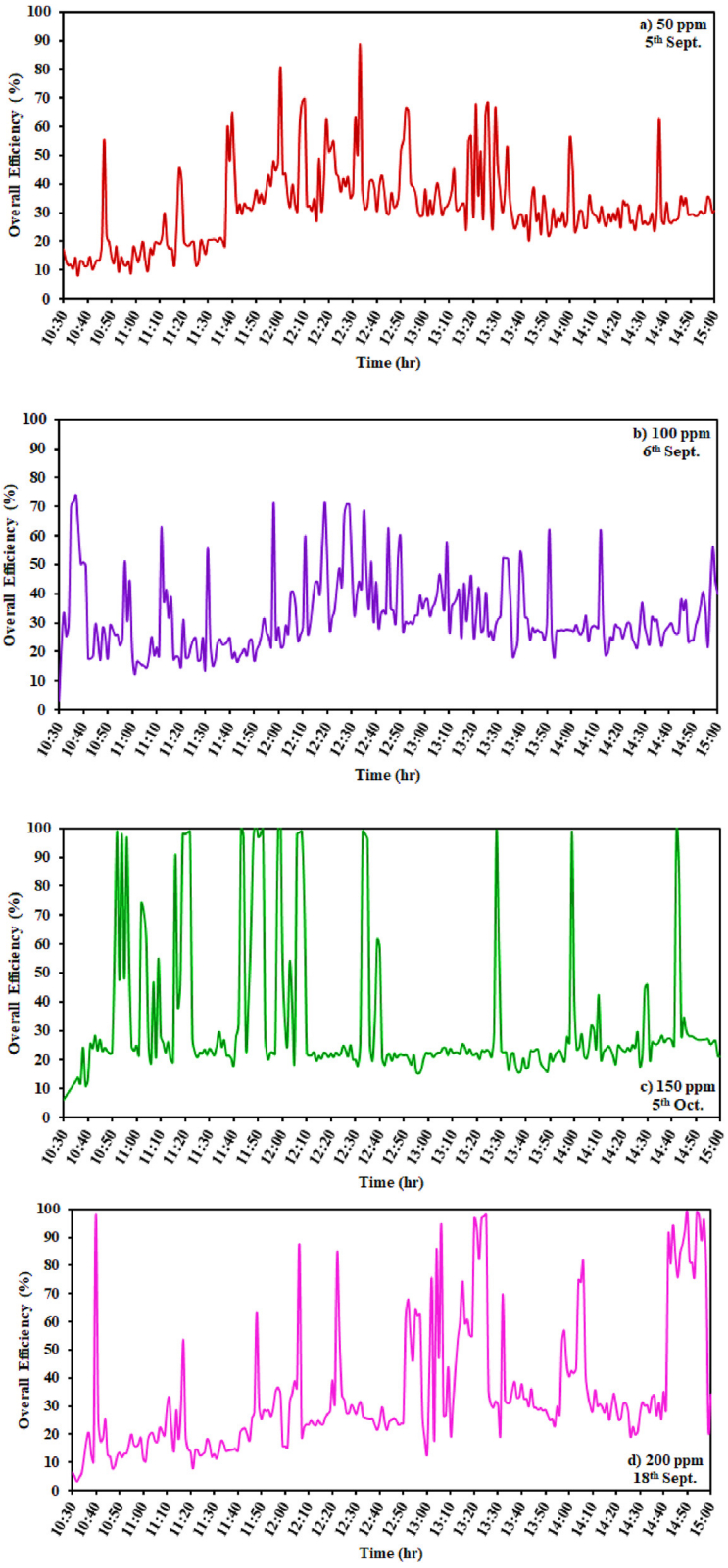

Fig. 15. The variation of overall efficiency over time for all studied cases.

attributable to the optical filter's capability to block unwanted solar radiation, which would otherwise heat the cell. Fig. 13 compares the average percent increase in electrical power and efficiency for all studied cases due to utilizing the nanofluid optical filter. As seen in Fig. 12, the percent enhancement in electrical power and efficiency shows a gradual rise from 88% to 89.3%–93% and 107.5%, respectively, with increasing nanofluid concentrations from 50 ppm to 200 ppm.

The temperature difference between nanofluid input and output impacts the thermal energy gain. The optical filter's thermal efficiency can thus be calculated as illustrated below (Huaxu et al., 2020):

$$\eta_{th} = \frac{\dot{m}_{nf} c_{p,nf} (T_o - T_i)}{I_{ab} A_{ab}} \quad (22)$$

Where $\dot{m}_{nf}$, $c_{p,nf}$, T_o, T_i are the nanofluid's mass flow rate, specific heat capacity, and outlet and inlet temperatures. I_{ab} the solar radiation intensity that reaches the filter. A_{ab} is the optical filter's surface area. The fluctuation of thermal efficiency with time for all tested cases at a constant average flow rate of 0.4 L/min is shown in Fig. 14. The following equation can give the system's overall efficiency (Huaxu et al., 2020):

$$\eta_{ov} = \frac{P_{PV} + \dot{m}_{nf} c_{p,nf} (T_o - T_i)}{I_{ab} A_{ab}} \quad (23)$$

Fig. 15 depicts the system's overall efficiency variations over time for all studied cases. Fig. 16 compares the filtered system's average electrical, thermal, and overall efficiencies for all studied cases. As shown in Fig. 16, although the electrical efficiency enhancement rises continuously with increasing concentration from 50 ppm to 200 ppm, the electrical efficiency rises from 7.1% at 50 ppm to 7.7% at 100 ppm and then declines to 6.7% and 6.2% at concentrations of 150 ppm and 200 ppm, respectively. Moreover, the thermal and overall efficiencies increase with increasing concentration, starting from 27.9% to 31.7% at 50 ppm to 31.4% and 34.6%, respectively.

Table 5 summarizes the main findings of the previous studies related to the current work. Many factors, including the concentration ratio, nanoparticle type, base fluid type, and PV semiconductor material, impact the thermal and electrical efficiency of PV/T systems, as shown in Table 5. It is noted that the effect of increasing the concentration on thermal efficiency using ZnO nanoparticles in glycol in the research done by Huaxu et al. (2020), which was previously mentioned in the introduction, agrees with what has been concluded in the current research using the same nanoparticle type in water, where the thermal efficiency increased with an increase in concentration from 11.2 ppm to 89.2 ppm by 47%. When the concentration was increased from 50 ppm to 200 ppm in the current study, the thermal efficiency increased from 27.9% to 31.40%. However, the study conducted by Zhang et al. (An et al., 2016a) showed a difference from the current study, as the thermal efficiency decreased with increasing the concentration of Cu_9S_5 in water. However, the effect of increasing the concentration on the electrical efficiency in the current study is different from that of the study done by Huaxu et al. (2020), as the electrical

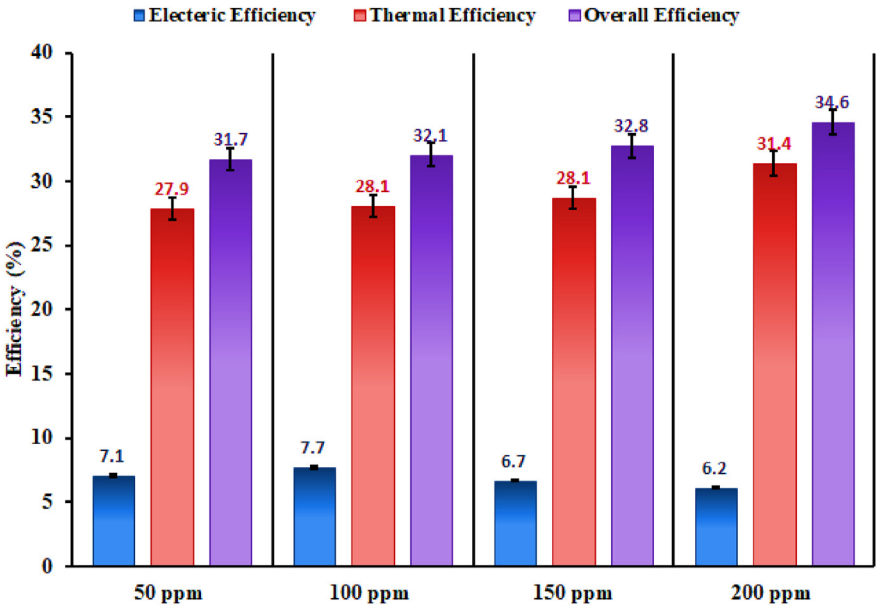

Fig. 16. The average performance of the filtered system for all studied cases.

Table 5. Related work comparison.

Related work	Concentration ratio	Nanoparticle type	Nanoparticle diameter (nm)	Base fluid	Nano-fluid concentration	The filtered wavelength range for PV cells (nm)	Electrical efficiency (%)	Thermal efficiency (%)	Overall efficiency (%)
Current work	4	ZnO	30	Water	50, 100, 150, and 200 ppm	Si (800–1100)	6.2–7.7	27.9–31.4	31.7–34.6
Huaxu et al. (2020) (Mojiri et al., 2013)	–	ZnO	–	Glycol	11.2–89.2 (ppm)	m-Si (400–1100)	13–15	7–11	21–25
Han et al. (2019) (Wang et al., 2022)	1	Ag	50	$CoSO_4$/Water	5.3–84.7 (ppm)	Si (600–1200)	5–16	25–40	30–55
He et al. (2019) (Xiao et al., 2016)	1	Ag @ TiO_2	23.6	Ethylene glycol /Water	50,100, and 200 (ppm)	Si (750–1100)	7–20	40–80	54–84
Brekke et al. (2018) (Huaxu et al., 2020)	14–26	Au (shelled by SiO_2) & In– TiO_2	5 & 75	Duratherm S	0.165 & 13.9 (ppm)	c-Si (600–1150)	12–19	53–70	38–70
Hjerrild et al. (2016) (Hjerrild et al., 2016)	10	Ag (shelled by SiO_2) & CNTs	6,13 and 17.5	Water	26 (ppm)	Si (700–1100)	5–18	15–55	30–60
An et al. (2016) (An et al., 2016a)	8.2&10.2	Cu_9S_5	60.2	Oleylamine	22.3, 44.6 and 89.2 (ppm)	m-Si (700–1100)	16–25	14–19	16–35
An et al. (2016) (Han et al., 2019)	10.2	Polypyrrole	13.68	Water	3.12, 6.25, and 12.5 (ppm)	P–Si	7–20	–	11–25

efficiency increased first in the current study from 7.1 to 7.7% by raising the concentration from 50 ppm to 100 ppm before decreasing to 6.2% by increasing the concentration to 200 ppm. In contrast, the electrical efficiency decreased with an increase in concentration in the study conducted by Huaxu et al. (2020). However, the electrical efficiency increased with the increase in concentration in the research conducted by Zhang et al. (An et al., 2016a).

There are anticipated challenges in scaling up the entire physical system because the technological economy is built on a large-scale system. One of these challenges is the potential for nanoparticle sedimentation after just a few hours of operation, which lowers the system's efficiency. To solve this issue, it is necessary to enclose the ultrasonic liquid processor in the nanofluid and use it frequently to keep particles from settling. One of the additional challenges is that using an increased quantity of liquid necessitates a higher pumping power than was used on a small scale. As a result, this power needs to be precisely computed, its quantity needs to be compared to the electrical energy and heat generated by the system, and efforts should be made to decrease it as much as possible. Finally, the possibility of a solar concentrator's shadow falling on the solar cells, which lowers the system's effectiveness, is one of the challenges that might arise when the system's scale is expanded. Thus, manual solar tracking needs to be performed frequently.

4.2. Conclusion

In order to prevent photovoltaic cells from overheating, spectral-splitting technology divides the sun's spectrum into two parts. The first part is immediately turned into electricity, and the second produces thermal energy. Numerous studies have shown that nanofluid is a very efficient absorbed liquid-based filter since it simultaneously functions as a heat transfer liquid and a spectral splitter. This study proposes a novel PV/T design that integrates a compound parabolic concentrator with a ZnO-water nanofluid that acts as a selective absorptive filter over the PV cell. Various tests were conducted to determine the effects of various ZnO-water nanofluid doses, including 50, 100, 150, and 200 ppm, on the system performance, and the average outcomes were then compared against a reference PV cell. The key findings are summarized as follows:

(1) The temperature percent reduction of filtered PV cells increases gradually with concentration, rising from 9.9% at a nanofluid concentration of 50 ppm to 10.7% at a concentration of 200 ppm.

(2) As the nanofluid's concentration rises from 50 ppm to 200 ppm, the average electrical power and efficiency percentage increase steadily from 88% to 89.3%–93% and 107.5%, respectively.
(3) The electrical efficiency increases from 7.1% at 50 ppm to 7.7% at 100 ppm and subsequently decreases to 6.7% and 6.2% at concentrations of 150 ppm and 200 ppm, respectively, even though the electrical efficiency enhancement constantly climbs with increasing concentration from 50 ppm to 200 ppm.
(4) With increasing concentration, the thermal and overall efficiencies gradually improve, going from 27.9% to 31.7% at 50 ppm to 31.4% and 34.6% at 200 ppm, respectively.

Author contribution

O. Elharoun: Study conception or design of the work, Data collection and tools, Investigation, Methodology, Statistical analysis, Data analysis and interpretation. M. Tawfik: Supervision, Visualization, Methodology, Drafting the article, Data analysis and interpretation, Critical revision of the article. Ibrahim I. El-Sharkawy: Supervision. E. Zeidan: Supervision, Drafting the article, Visualization, Final approval of the version to be published.

Conflict of interest

There are no conflicts of interest.

Nomenclature

A	Area (m^2)
CR	Concentration ratio (–)
c_p	Specific heat capacity (J/kg K)
D	Diameter (m)
e	Thickness (m)
f	Focal length (m)
H	Height (m)
I	Radiation intensity (W/m^2), Current (A)
κ	Absorption index (–)
m	Mass (kg)
$\dot{m}$	Mass flow rate (kg/s)
n	Refraction index (–)
P	Power (W)
R	Complex refractive index (–)
T	Temperature (K)
V	Voltage (V)
W	Width (m)

Greek Letters

η	Efficiency
θ_i	Incidence angle
λ	Wavelength (nm)
σ	Extinction coefficient

Subscripts

ab	Absorber
ac	Acrylic
ap	Aperture
abs	Absorption
bf	Base fluid
CPC	Compound parabolic concentrator
mp	Maximum power
nf	Nanofluid
np	Nanoparticles
ov	Overall
oc	Open circuit
of	Optical filter
ref	Reference
sc	Short circuit, Scattering
T	Truncated
ρ	Reflectivity, density (kg/m^3)
$\varnothing_v$	Volume fraction
θ_a	Half-acceptance angle
τ	Transmittance

References

Adam, S.A., Ju, X., Zhang, Z., El-samie, M.M.A., 2019. Theoretical investigation of different CPVT configurations based on liquid absorption spectral beam filter. Energy 189, 116259. https://doi.org/10.1016/j.energy.2019.116259.

An, W., Zhang, J., Zhu, T., Gao, N., 2016a. Investigation on a spectral splitting photovoltaic/thermal hybrid system based on polypyrrole nanofluid: preliminary test. Renew. Energy 86, 633–642. https://doi.org/10.1016/j.renene.2015.08.080.

An, W., Wu, J., Zhu, T., Zhu, Q., 2016b. Experimental investigation of a concentrating PV/T collector with Cu9S5 nanofluid spectral splitting filter. Appl. Energy 184, 197–206. https://doi.org/10.1016/j.apenergy.2016.10.004.

An, W., Chen, L., Liu, T., Qin, Y., 2018. Enhanced solar distillation by nanofluid-based spectral splitting PV/T technique: preliminary experiment. Sol. Energy 176, 146–156. https://doi.org/10.1016/j.solener.2018.10.029.

Bahaidarah, H.M., Tanweer, B., Gandhidasan, P., Ibrahim, N., Rehman, S., 2014. Experimental and numerical study on non-concentrating and symmetric unglazed compound parabolic photovoltaic concentration systems. Appl. Energy 136, 527–536. https://doi.org/10.1016/j.apenergy.2014.09.060.

Crisostomo, F., Hjerrild, N., Mesgari, S., Li, Q., Taylor, R.A., 2017. A hybrid PV/T collector using spectrally selective absorbing nanofluids. Appl. Energy 193, 1–14. https://doi.org/10.1016/j.apenergy.2017.02.028.

Digital Thermometer (DS18B20-PAR). Available online: https://www.mouser.com/datasheet/2/256/DS18B20-PAR-315769.pdf. (Accessed 26 September 2022).

Hale, G.M., Querry, M.R., 1973. Optical constants of water in the 200-Nm to 200-Mm wavelength region. Appl. Opt. 12, 555. https://doi.org/10.1364/AO.12.000555.

Han, X., Chen, X., Wang, Q., Alelyani, S.M., Qu, J., 2019. Investigation of CoSO4-based Ag nanofluids as spectral beam splitters for hybrid PV/T applications. Sol. Energy 177, 387–394. https://doi.org/10.1016/j.solener.2018.11.037.

He, Y., Hu, Y., Li, H., 2019. An Ag@TiO2/Ethylene Glycol/water solution as a nanofluid-based beam splitter for photovoltaic/thermal applications in cold regions. Energy Convers. Manag. 198, 111838. https://doi.org/10.1016/j.enconman.2019.111838.

High Precision PVC Water Flow Sensor YF-S401. Available online: https://www.epitran.it/ebayDrive/datasheet/YF-S401.pdf. (Accessed 26 September 2022).

Hjerrild, N.E., Mesgari, S., Crisostomo, F., Scott, J.A., Amal, R., Taylor, R.A., 2016. Hybrid PV/T enhancement using selectively absorbing Ag–SiO2/Carbon nanofluids. Sol. Energy Mater. Sol. Cells 147, 281–287. https://doi.org/10.1016/j.solmat.2015.12.010.

Huaxu, L., Fuqiang, W., Dong, L., Jie, Z., Jianyu, T., 2019. Optical properties and transmittances of ZnO-containing nanofluids in spectral splitting photovoltaic/thermal systems. Int. J. Heat Mass Tran. 128, 668–678. https://doi.org/10.1016/j.ijheatmasstransfer.2018.09.032.

Huaxu, L., Fuqiang, W., Dong, Z., Ziming, C., Chuanxin, Z., Bo, L., Huijin, X., 2020. Experimental investigation of cost-effective ZnO nanofluid based spectral splitting CPV/T system. Energy 194, 116913. https://doi.org/10.1016/j.energy.2020.116913.

Jing, D., Song, D., 2017. Optical properties of nano fluids considering particle size distribution : experimental and theoretical investigations. Renew. Sustain. Energy Rev. 78, 452–465. https://doi.org/10.1016/j.rser.2017.04.084.

Jing, D., Hu, Y., Liu, M., Wei, J., Guo, L., 2015. Preparation of highly dispersed nanofluid and CFD study of its utilization in a concentrating PV/T system. Sol. Energy 112, 30–40. https://doi.org/10.1016/j.solener.2014.11.008.

Li, H., He, Y., Wang, C., Wang, X., Hu, Y., 2019. Tunable thermal and electricity generation enabled by spectrally selective absorption nanoparticles for photovoltaic/thermal applications. Appl. Energy 236, 117–126. https://doi.org/10.1016/j.apenergy.2018.11.085.

Manoharan, C., Pavithra, G., Bououdina, M., Dhanapandian, S., Dhamodharan, P., 2016. Characterization and study of antibacterial activity of spray pyrolysed ZnO:Al thin films. Appl. Nanosci. 6, 815–825. https://doi.org/10.1007/s13204-015-0493-8.

Max471/Max472. Available online: https://datasheets.maximintegrated.com/en/ds/MAX471-MAX472.pdf. (Accessed 26 September 2022).

Mojiri, A., Taylor, R., Thomsen, E., Rosengarten, G., 2013. Spectral beam splitting for efficient conversion of solar energy—a review. Renew. Sustain. Energy Rev. 28, 654–663. https://doi.org/10.1016/j.rser.2013.08.026.

Molded Plastic Aspheric Lenses. Available online: https://www.thorlabs.com/newgrouppage9.cfm?objectgroup_ID=16. (Accessed 27 September 2022).

NREL(Reference Air Mass 1.5 Spectra). Available online: https://www.nrel.gov/grid/solar-resource/spectra-am1.5.html. (Accessed 7 December 2022).

Otanicar, T.P., Phelan, P.E., Golden, J.S., 2009. Optical properties of liquids for direct absorption solar thermal energy systems. Sol. Energy 83, 969–977. https://doi.org/10.1016/j.solener.2008.12.009.

Otanicar, T., Dale, J., Orosz, M., Brekke, N., DeJarnette, D., Tunkara, E., et al., 2018. Experimental evaluation of a prototype hybrid CPV/T system utilizing a nanoparticle fluid absorber at elevated temperatures. Appl. Energy 228, 1531–1539. https://doi.org/10.1016/j.apenergy.2018.07.055.

Rodrigues Fernandes, M., Schaefer, L.A., 2019. Long-term environmental impacts of a small-scale spectral filtering concentrated photovoltaic-thermal system. Energy Convers. Manag. 184, 350–361. https://doi.org/10.1016/j.enconman.2019.01.026.

Royanian, S., Abdolahzadeh Ziabari, A., Yousefi, R., 2020. Efficiency enhancement of ultra-thin cigs solar cells using bandgap grading and embedding Au plasmonic nanoparticles. Plasmonics 15, 1173–1182. https://doi.org/10.1007/s11468-020-01138-2.

Saroha, S., Mittal, T., Modi, P.J., Bhalla, V., Khullar, V., Tyagi, H., et al., 2015. Theoretical analysis and testing of nanofluids-based solar photovoltaic/thermal hybrid collector. J. Heat Tran. 137, 1–8. https://doi.org/10.1115/1.4030228.

SOLAR POWER METER Model : SPM-1116SD. https://www.sunwe.com.tw/lutron/SPM-1116SD.pdf. (Accessed 26 September 2022).

Taylor, R.A., Phelan, P.E., Otanicar, T.P., Adrian, R., Prasher, R., 2011. Nanofluid optical property characterization: towards efficient direct absorption solar collectors. Nanoscale Res. Lett. 6, 1–11. https://doi.org/10.1186/1556-276X-6-225.

Taylor, R.A., Otanicar, T., Rosengarten, G., 2012. Nanofluid-based optical filter optimization for PV/T systems. Light Sci. Appl. 1, e34. https://doi.org/10.1038/lsa.2012.34 e34.

Vane Anemometer (Testo 416). https://static-int.testo.com/media/93/18/9dd27c5c3221/testo-416-data-sheet.pdf. (Accessed 26 September 2022).

Vidhya, R., Balakrishnan, T., Suresh Kumar, B., 2021. Investigation on thermophysical properties of zinc oxide nanofluid for heat transfer applications. Mater. Today: Proc. 58, 789–794. https://doi.org/10.1016/j.matpr.2021.09.008.

Wang, G., Zhang, Z., Jiang, T., Lin, J., Chen, Z., 2022. Thermodynamic and optical analyses of a novel solar CPVT system based on parabolic trough concentrator and nanofluid spectral filter. Case Stud. Therm. Eng. 33, 101948. https://doi.org/10.1016/j.csite.2022.101948.

Waterproof Temperature Sensor Cable (DS18B20). Available online: https://www.terraelectronica.ru/pdf/show?pdf_file=%2Fz%2FDatasheet%2F1%2F1420644897.pdf. (Accessed 26 September 2022).

Xiao, T.P., Cifci, O.S., Bhargava, S., Chen, H., Gissibl, T., Zhou, W., et al., 2016. Diffractive spectral-splitting optical element designed by adjoint-based electromagnetic optimization and fabricated by femtosecond 3D direct laser writing. ACS Photonics 3, 886–894. https://doi.org/10.1021/acsphotonics.6b00066.

Yazdanifard, F., Ameri, M., Taylor, R.A., 2020. Numerical modeling of a concentrated photovoltaic/thermal system which utilizes a PCM and nanofluid spectral splitting. Energy Convers. Manag. 215, 112927. https://doi.org/10.1016/j.enconman.2020.112927.

Zarandi, M.B., Bioki, H.A., 2017. Effects of cobalt doping on optical properties of ZnO thin films deposited by sol-gel spin coating technique. J. Optoelectron. Nanostruct. 2, 33–44.

Zheng, H., 2017. Solar energy utilization and its collection devices. In: Solar Energy Desalination Technology, vols. 47–171. Elsevier, 9780128054116. https://doi.org/10.1016/B978-0-12-805411-6.00002-6.